Phase separation in the Edwards model

S. Ejima,[1] S. Sykora,[2] K. W. Becker,[3] and H. Fehske[1]
[1]*Institut für Physik, Ernst-Moritz-Arndt-Universität Greifswald, 17487 Greifswald, Germany*
[2]*Institute for Theoretical Solid State Physics, IFW Dresden, 01069 Dresden, Germany*
[3]*Institut für Theoretische Physik, Technische Universität Dresden, 01062 Dresden, Germany*
(Received 13 August 2012; published 25 October 2012)

The nature of charge transport within a correlated background medium can be described by spinless fermions coupled to bosons in the model introduced by Edwards. Combining numerical density matrix renormalization group and analytical projector-based renormalization methods, we explore the ground-state phase diagram of the Edwards model in one dimension. Below a critical boson frequency, any long-range order disappears and the system becomes metallic. If the charge carriers are coupled to slow quantum bosons, the Tomonaga-Luttinger liquid is attractive and finally makes room for a phase separated state, just as in the t-J model. The phase boundary separating the repulsive from the attractive Tomonaga-Luttinger liquid is determined from long-wavelength charge correlations, whereas fermion segregation is indicated by a vanishing inverse compressibility. On approaching phase separation, the photoemission spectra develop strong anomalies.

DOI: 10.1103/PhysRevB.86.155149 PACS number(s): 71.10.Hf, 71.30.+h, 71.10.Fd

I. PROBLEM

The Edwards fermion-boson model[1,2] constitutes a paradigmatic model for the theoretical description of quantum transport in solids. Charge transport normally takes place in the presence of some background medium.[3] Examples for such a "background" could be a spin-, charge-, or orbital-ordered lattice,[4,5] but also a sequence of chemical side groups along the transport path, a deformable medium, or even a heat bath might be possible. In all these cases, the transfer of the charge carriers will be strongly influenced by fluctuations, which may exist in the background medium. The other way around, the properties of the background are quite often determined by the motion of the particle itself.

Correlations inherent in such a complex interactive system are mimicked by a boson-affected hopping of spinless fermionic particles in the Edwards model. It reads

$$H = -t_b \sum_{\langle i,j \rangle} f_j^\dagger f_i (b_i^\dagger + b_j) - \lambda \sum_i (b_i^\dagger + b_i) + \omega_0 \sum_i b_i^\dagger b_i \,. \tag{1}$$

Every time a fermion $f_i^{(\dagger)}$ hops, it creates or absorbs a boson $b_i^{(\dagger)}$ of energy ω_0 at the sites it leaves or enters. Such an excitation or deexcitation corresponds to a local "distortion" of the background. Because of quantum fluctuations, the distortions are able to relax ($\propto \lambda$). The physically most interesting regimes in this setting are those of vanishing fermion density and of a half-filled band, representing doped Mott insulators, polaronic organics, and charge-density-wave (CDW) systems[6–9] with possible relevance to high-T_c superconductors,[10,11] colossal magnetoresistive manganites,[12–14] carbon nanotubes,[15,16] graphene,[17,18] and CDW transition metal complexes,[19,20] respectively. However, the Edwards model also reveals fascinating properties over the whole density range.

On these grounds, the main goal of the present work is to pinpoint the ground-state phase diagram of the one-dimensional (1D) Edwards model as a function of the band filling n. Thereby, we demonstrate that this model indeed captures a number of very interesting phenomena, including, e.g., electronic phase separation (PS). To obtain reliable information about the ground-state and spectral properties of the model in the thermodynamic limit, we employ numerical pseudosite density-matrix renormalization group (DMRG) and dynamical DMRG (DDMRG) techniques (supplemented by a careful finite-size scaling procedure; for details, see Refs. 9 and 21–24), in combination with the analytical projective renormalization method (PRM).[25,26]

So far the 1D Edwards model has been solved exactly by numerical approaches for two cases.[22,24,27] The first, in no way trivial, case concerns just a single particle on an infinite lattice, where—depending on the model parameters—transport appears to be quasifree, diffusive, or boson-assisted.[6,28] When strong correlations develop at small λ and large ω_0, the background becomes "stiff" and the spinless particle's motion resembles those of a hole in an antiferromagnetic spin background,[29,30] as known from the t-J model. Interestingly, the Edwards model allows for so-called Trugman paths[31] in a 1D setting (Trugman paths usually unwind the string of misaligned spins a mobile hole leaves behind in two dimensions). The second case is half-filling, $n = 1/2$. Here a metal-insulator transition has been proven to exist: For small λ and large ω_0, the repulsive Tomonaga-Luttinger liquid (TLL) gives way to a CDW.[7,8] The CDW constitutes a few-boson state that typifies a Mott-Hubbard insulator rather than a Peierls state (normally established by the softening of a boson mode).

II. THEORETICAL RESULTS

A. Ground-state properties

The situation at finite density n ($n \neq 1/2$) is much less understood. By analogy with the t-J model, one might expect that the system is metallic for $0 < n < 1/2$, at least if the background is not too stiff. If so, the next question will be whether the Edwards model might support the pairing of electrons in a certain parameter regime (λ,ω_0). Apparently a second electron, following the path of a first one, can take advantage of the background excitations (bosons) left behind

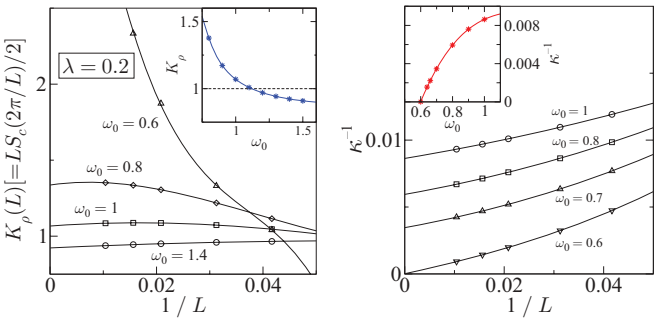

FIG. 1. (Color online) Finite-size scaling of the TLL parameter K_ρ (left panel) and inverse compressibility κ^{-1} (right panel) for the 1D Edwards model with $\lambda = 0.2$ at $n = 1/8$. Insets show the variation with ω_0 of the $L \to \infty$ extrapolated values. Results are obtained by DMRG for a lattice with L sites and OBC. In all DMRG runs, we take into account up to $n_b = 4$ bosonic pseudosites and determine n_b by the requirement that the local boson density of the last pseudosite is less than 10^{-6} for all j. Using selectively $n_b = 5$, we controlled that convergence is truly achieved. Furthermore, we keep up to $m = 1200$ density-matrix eigenstates in the renormalization steps to ensure that the discarded weight is smaller than 10^{-8}.

by the first electron. This acts like an effective attractive interaction. If this attraction completely dominates the kinetic energy, the system might even phase-separate into particle-enriched and particle-depleted regions.[32] Since the Edwards model is not particle-hole symmetric, it is a moot point whether a corresponding hole pairing mechanism is at play also for $1/2 < n < 1$.

To address these problems, we analyze the charge correlations existing in the ground state of the 1D Edwards model. First, we calculate the charge structure factor

$$S_c(q) = \frac{1}{L} \sum_{j,l} e^{iq(j-l)} \langle (f_j^\dagger f_j - n)(f_l^\dagger f_l - n) \rangle \qquad (2)$$

for a system with N fermions, L sites, and open boundary conditions (OBCs). So the particle density is $n = N/L$ and the momenta $q = 2\pi s/L$ with integers $0 < s < L$. The TLL charge exponent is proportional to the slope of $S_c(q)$ in the long-wavelength limit $q \to 0^+$ (cf. Refs. 33 and 34):

$$K_\rho = \pi \lim_{q \to 0} \frac{S_c(q)}{q} . \qquad (3)$$

Then, $K_\rho > 1$ ($K_\rho < 1$) characterizes an attractive (repulsive) TLL for our spinless fermion transport model (1), and $K_\rho = 1/2$ will define a metal-insulator transition point at $n = 1/2$.[35] That the finite-size scaling of $S_c(q)$ and K_ρ works well has been demonstrated for the half-filled band case.[8] Secondly, in order to comprise potential PS, we determine the finite-size equivalent of the charge compressibility,[36]

$$\kappa = \frac{L}{N^2} \left[\frac{E_0(N+2) + E_0(N-2) - 2E_0(N)}{4} \right]^{-1} , \qquad (4)$$

with $E_0(N)$ being the ground-state energy for N electrons on L sites. An infinite compressibility signals the formation of a PS state.

Figure 1 demonstrates that all this works in practice. Exemplarily choosing $n = 1/8$ and $\lambda = 0.2$, we show how the

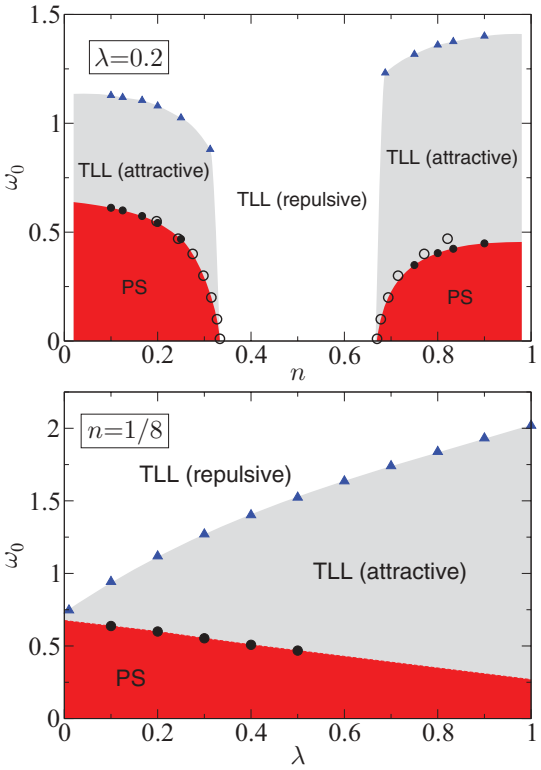

FIG. 2. (Color online) Ground-state phase diagram of the 1D Edwards model, showing repulsive TLL ($K_\rho < 1$), attractive TLL ($K_\rho > 1$), and PS ($\kappa^{-1} = 0$) regions. The phase boundaries were obtained by DMRG (filled symbols) in the course of a careful finite-size scaling analysis and for the infinite system directly by PRM (open symbols). The upper panel displays the phase diagram as a function of n, varying ω_0 at fixed $\lambda = 0.2$; the lower panel gives the phase diagram in the λ-ω_0 plane for fixed density $n = 1/8$.

TLL exponent K_ρ and the inverse compressibility κ^{-1} scale with increasing system size at various ω_0. The transition point between a repulsive TLL—obviously realized at $\omega_0 > \omega_{0,c1}$ when excitations of the background are energetically rather costly—and an attractive TLL at smaller ω_0 can be read off from the inset [depicting the extrapolations $K_\rho(L \to \infty)$] to be $\omega_{0,c1}(\lambda = 0.2) \simeq 1.118$. Reducing ω_0 further, in the attractive TLL phase, a dramatic increase in K_ρ is observed at $\omega_{0,c2} \simeq 0.6$. Our inverse compressibility data indicate that at this point, the attraction among the particles becomes so strong that the system shows PS, i.e., $\kappa^{-1} = 0$ for $\omega_0 < \omega_{0,c2}$.

Proceeding in the same manner for different values of n and λ, and, respectively, ω_0, we can map out the phase diagram of the 1D Edwards model. The outcome is displayed in Fig. 2. Let us first consider the case of a not too small boson relaxation ($\propto \lambda$), which ensures that the system is metallic for large ω_0 in the whole density regime. Then, as the upper panel of Fig. 2 shows, depending on n we find up to three different regimes: For small and large particle densities, a repulsive TLL, an attractive TLL, and a PS state appear in sequence as the energy of the bosons is lowered. In contrast, around half-filling only the repulsive TLL exists. At this point, we would like to remind the reader that at half-filling, for smaller values of λ ($\lambda < \lambda_c$), a CDW is formed for $\omega_0 > \omega_{0,c}$.[8] Our unbiased DMRG calculations give no evidence for any other phases. Note that

the behavior in the low-density regime is consistent with what is found for the 1D t-J model,[36,37] where the holes correspond to the spinless fermions in the Edwards model. As mentioned before, the phase diagram is not symmetric with respect to $n = 1/2$. This is because the hopping of a hole (missing electron) to a neighboring site creates in the Edwards model a boson at the arrival site and not on the departure site, as in the motion of a single particle. Since this boson can be destroyed immediately when the hole makes a further hop, there is no string effect and a few holes propagate more easily than a few electrons. Hence the background at fixed ω_0 and λ appears to be less stiff for $n \lesssim 1$ than for $n \gtrsim 0$ and, as a result, the boundary between the repulsive and attractive TLL is shifted to larger values of $\omega_{0,c1}$. Contrariwise, since carriers will be less mobile in a state with charge separation, the boundary between the attractive TLL and the PS state $\omega_{0,c2}$ is shifted to smaller values if one compares the corresponding results at high and low carrier density.

We next consider a fixed particle density $n = 1/8$ and track the phase boundaries in the λ-ω_0 plane; see the lower panel of Fig. 2. The repulsive TLL established for large ω_0 is strongly renormalized if the ability of the background to relax is low. For example, we find $K_\rho = 0.527$ for $\omega_0 = 2$ at $\lambda = 0.01$. Lowering ω_0 for such a stiff background, the transition to the PS state happens almost instantaneously with a narrow intervening attractive TLL state; at $\lambda = 0.01$ we have $\omega_{0,c1} \simeq 0.747$ and $\omega_{0,c2} \simeq 0.672$. If we fix, on the other hand, $\omega_0 = 2$ and increase λ, we observe a strong enhancement of K_ρ in the interval $0 < \lambda < 0.3$ ($K_\rho = 0.767$, 0.879, and 0.932 for $\lambda = 0.1, 0.2$, and 0.3, respectively), followed by a very gradual increase until the transition to the attractive TLL takes place at about $\lambda_{c1} \simeq 1$. Obviously, the region where the attractive TLL (PS state) constitutes the ground state expands (shrinks) as λ gets larger, which can be traced back to the subtle competition between kinetic energy and charge segregation effects.

To gain deeper insight into the different mechanisms at play, we analyze the variation of the local fermion $[n_j^f = \langle f_j^\dagger f_j \rangle]$ and boson $[n_j^b = \langle b_j^\dagger b_j \rangle]$ densities in real space. In Fig. 3, we show both density profiles for $n = 1/8$ and characteristic values of λ and ω_0, implementing repulsive TLL, attractive TLL, and PS states. In the metallic regime, the OBCs lead to Friedel oscillations in the particle density. These oscillations are especially pronounced for the repulsive TLL [Fig. 3(a)], and they will be even stronger for $\omega_0 = 2$ (not shown), where the number and fluctuations of the bosons is reduced. Note that the Friedel oscillations caused by the OBC will be algebraically reduced if we move for very large systems toward the central part of the chain. If we enter the attractive TLL regime by increasing λ at fixed ω_0, the Friedel oscillation will be smeared out [Fig. 3(b)]. Thereby, the number of oscillations stays constant, which means that a pairing of electrons does not occur. This is an important difference from the spinful 1D t-J model, where a recent DMRG study reveals that the number of Friedel oscillations is halved (by increasing J), corresponding to half the number of particles, which indicates pairing.[37] Next, lowering ω_0 to a point where PS sets in, the particle density oscillations vanish; see Fig. 3(c). There, just above the PS boundary, no evidence is found for the clustering of multiple particles in several groups. This agrees with the findings for the 1D t-J model.[37] Once we are deep inside the

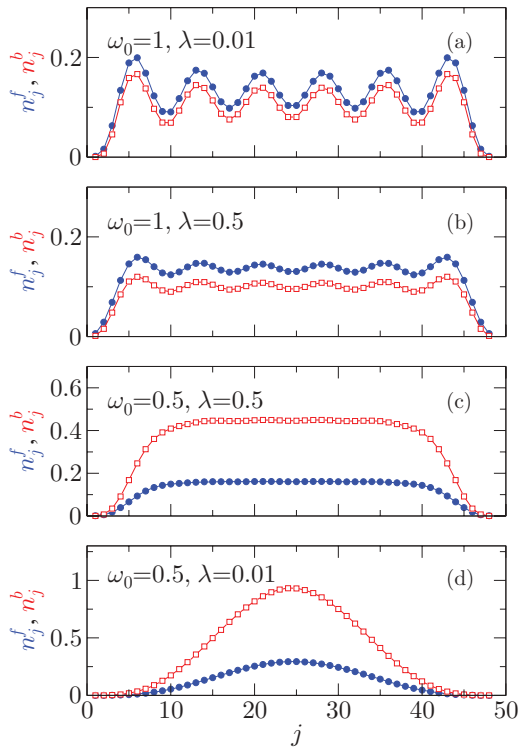

FIG. 3. (Color online) Local particle (filled circles) and boson (open squares) densities for the 1D Edwards model with $n = 1/8$, calculated for a 48-site system with OBC at various λ and ω_0.

PS region, a density distribution results, where a single island of particles at the central part of the system appears, leaving a sizable number of almost empty sites at both ends of the chain [see Fig. 3(d)]. Looking at the bosonic degrees of freedom, we see that the strong attraction among these particles is mediated by a boson cloud covering the electron-rich region. As a result, the kinetic fluctuations will be strongly quenched.

It is all but impossible to comprise by DMRG the large number of bosons and the strong bosonic fluctuations, which appear at still smaller ω_0 in the Edwards model, simply because the dimension of the Hilbert space increases dramatically. To access the low-ω_0 regime and reconfirm the DMRG phase boundaries obtained for the 1D Edwards model at larger values of ω_0, we employ the analytical PRM approach.[25] The basic idea of the PRM approach is to construct—performing a sequence of discrete unitary transformations and eliminating all transitions with energy larger than a given cutoff energy—an effective noninteracting Hamiltonian $\tilde{H}$ with renormalized parameters (in the limit of vanishing cutoff energy). For the metallic state of the Edwards model, in momentum space, it takes the form

$$\tilde{H} = \sum_k \tilde{\varepsilon}_k f_k^\dagger f_k + \sum_q \tilde{\omega}_q b_q^\dagger b_q + \tilde{E}, \tag{5}$$

where the renormalization equations for $\tilde{\varepsilon}_k$ and $\tilde{\omega}_q$ have been derived in Ref. 26 (for the half-filled band case). To fix the boundary between metallic and PS states, we (i) solve the renormalization equations at a given E_F in the TLL phase, (ii) determine the corresponding fermion density n, and (iii) slightly vary E_F (to get closer to the PS instability), determine n, and repeat the whole procedure self-consistently

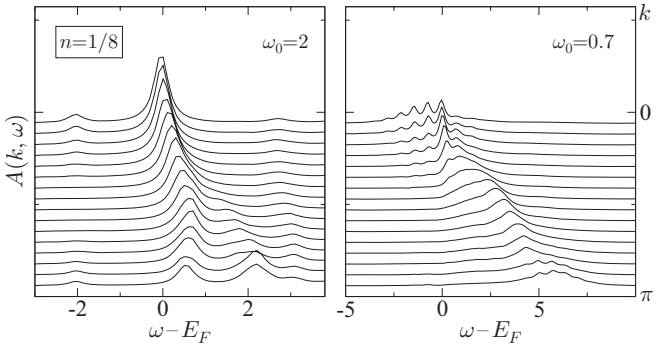

FIG. 4. Line-shape of the single-particle spectral function $A(k,\omega)$ for the 1D Edwards model with $\lambda = 0.2$ at $n = 1/8$. Results are obtained by DDMRG for a 16-site chain with quasimomenta $k = \pi s/(L+1)$, using a broadening $\eta = 0.2$.

until the functional dependence of n on E_F is established. A vanishing inverse compressibility can then be read off from a sudden jump of n under a tiny variation of E_F or, the other way around, if a plateau in the E_F versus n plot appears. The transition points, determined in the manner described, were inserted in Fig. 2 to complete the ground-state phase diagram in the n-ω_0 plane. Whenever points can be compared, we find a remarkable agreement between our DMRG and PRM data. The deviation of the PRM data at larger particle densities $n \gtrsim 0.75$ results from uncertainties in fixing the jump of n under E_F variation. Here we should trust in the DMRG phase boundary.

B. Spectral properties

Let us finally discuss the single-particle spectrum of the 1D Edwards model. The single-particle excitations associated with the injection (+) or emission (−) of an electron with wave vector k,

$$A^{\pm}(k,\omega) = \sum_m |\langle\psi_m^{\pm}|f_k^{\pm}|\psi_0\rangle|^2\,\delta(\omega \mp \omega^{\pm}), \qquad (6)$$

can be computed by DDMRG,[23,24] where $f_k^+ = f_k^\dagger$, $f_k^- = f_k$, $|\psi_0\rangle$ is the ground state of an L-site system in the N-particle sector, and $|\psi_m^{\pm}\rangle$ denotes the mth excited states in the $(N \pm 1)$-particle sectors with excitation energies $\omega_m^{\pm} = E_m^{\pm} - E_0$.

Within PRM, we find for the photoemission part

$$\begin{aligned} A^-(k,\omega) = {} & \tilde{\alpha}_k^2\,\tilde{n}_k^f\,\delta(\omega - \tilde{\varepsilon}_k) \\ & + \sum_q \tilde{\beta}_{k,q}^2\,(1+\tilde{n}_q^b)\tilde{n}_{k+q}^f\,\delta(\omega + \tilde{\omega}_q - \tilde{\varepsilon}_{k+q}) \\ & + \sum_q \tilde{\gamma}_{k,q}^2\,\tilde{n}_q^b\tilde{n}_{k-q}^f\,\delta(\omega - \tilde{\omega}_q - \tilde{\varepsilon}_{k-q}), \end{aligned} \qquad (7)$$

where $\tilde{n}_q^f$ ($\tilde{n}_q^b$) are the fermion (boson) occupation numbers in momentum space calculated with the renormalized Hamiltonian $\tilde{H}$. The coefficients $\tilde{\alpha}_k^2$, $\tilde{\beta}_{k,q}^2$, and $\tilde{\gamma}_{k,q}^2$ follow from renormalization equations.[26] Taking the corresponding expression for $A^+(k,\omega)$, the sum rule $\int_\infty^\infty d\omega[A^+(k,\omega) + A^-(k,\omega)] = 1$ is fulfilled.

Figure 4 gives the combined photoemission spectrum, $A(k,\omega) = A^+(k,\omega) + A^-(k,\omega)$, as obtained by DDMRG for quasimomenta k. In the repulsive TLL regime (left panel, $\omega_0 = 2$), we find a rather coherent signal with comparable spectral weight for all k values $k \lesssim \pi/2$. For larger k, excitations with at least one additional ω_0 boson involved become important (recall that both initial N-particle- and target $(N \pm 1)$-particle states are multiboson states with a momentum being the total momentum of electrons and bosons). The spectrum in the attractive TLL phase (right panel, $\omega_0 = 0.7$) shows a sharp absorption signal in the vicinity of k_F only. Here the (inverse) photoemission spectrum for $k < k_F$ ($k > k_F$) exhibits a few absorption maxima at multiples of the boson energy. Obviously, due to the smaller ω_0, here the dynamics of the system becomes dominated by bosonic fluctuations.

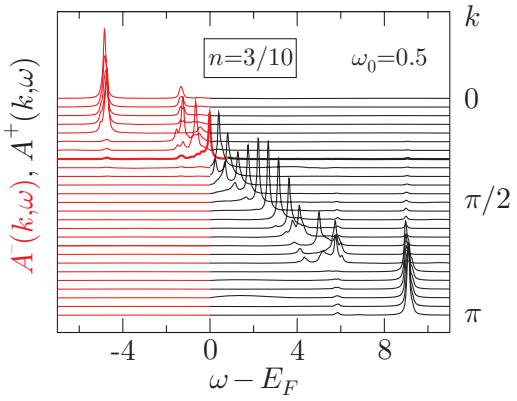

FIG. 5. (Color online) PRM (inverse) photoemission spectrum $[A^+(k,\omega)]$ $A^-(k,\omega)$ for the Edwards model with $\lambda = 0.2$, $n = 3/10$. The bold line marks the signal at the Fermi momentum $k_F = 0.3\pi$.

The (inverse) photoemission close to the transition to the PS state is depicted in Fig. 5, as calculated by PRM for $\omega_0 = 0.5$. Here the almost dispersionless signal for $k \leqslant 0.212\pi$ ($k \geqslant 0.788\pi$) is a precursor of the PS instability. As we noted above, E_F does not show any variation with n if n is smaller (larger) than the lower (upper) critical density n_{c2} for PS. Since in the PRM derivation of $A^{\pm}(k,\omega)$ terms with two (and more) bosonic creation or annihilation operators were neglected,[26] the photoemission spectrum of Fig. 5 does not feature the multiboson related signatures found within a DDMRG treatment.

III. CONCLUSIONS

To summarize, the combination of analytical (PRM) and numerical (DMRG) approaches permits the precise determination of the ground-state phase diagram of the 1D Edwards model in the whole parameter regime. In the low- and high-density regions, the attraction between the particles mediated by the bosonic degrees of freedom representing the background medium might become so strong that electronic PS sets in. In the remaining region, the system realizes a TLL or, at $n = 1/2$, possibly even a truly long-range ordered CDW state. Depending on the properties of the background medium, the TLL might be attractive or repulsive. The richness of the phase diagram is remarkable. The model captures important features of Holstein, t-J, Hubbard, and Falicov-Kimball type models.[6–9,38] Since the Edwards model is one of the simplest models for studying transport in low-dimensional systems,

an inspection of its predictions with ultracold fermion/boson quantum gases,[39] as, e.g., carried out for the 1D t-J model,[40] would be of great interest.

ACKNOWLEDGMENT

This work was supported by DFG through SFB 652.

[1] D. M. Edwards, Physica B **378-380**, 133 (2006).
[2] D. M. Edwards, S. Ejima, A. Alvermann, and H. Fehske, J. Phys.: Condens. Matter **22**, 435601 (2010).
[3] M. Berciu, Physics **2**, 55 (2009).
[4] L. G. L. Wegener and P. B. Littlewood, Phys. Rev. B **66**, 224402 (2002).
[5] K. Wohlfeld, A. M. Oleś, and P. Horsch, Phys. Rev. B **79**, 224433 (2009).
[6] A. Alvermann, D. M. Edwards, and H. Fehske, Phys. Rev. Lett. **98**, 056602 (2007).
[7] G. Wellein, H. Fehske, A. Alvermann, and D. M. Edwards, Phys. Rev. Lett. **101**, 136402 (2008).
[8] S. Ejima, G. Hager, and H. Fehske, Phys. Rev. Lett. **102**, 106404 (2009).
[9] S. Ejima and H. Fehske, Phys. Rev. B **80**, 155101 (2009).
[10] I. G. Bednorz and K. A. Müller, Z. Phys. B **64**, 189 (1986).
[11] E. Dagotto, Rev. Mod. Phys. **66**, 763 (1994).
[12] G. H. Jonker and J. H. van Santen, Physica **16**, 337 (1950).
[13] E. Dagotto, *Nanoscale Phase Separation and Colossal Magnetoresistance: The Physics of Manganites and Related Compounds* (Springer, Heidelberg, 2003).
[14] A. Weiße and H. Fehske, New J. Phys. **6**, 158 (2004).
[15] R. Saito, G. Dresselhaus, and M. S. Dresselhaus, *Physical Properties of Carbon Nanotubes* (Imperial College, London, 1998).
[16] H. Mousavi and M. Bagheri, Physica E **44**, 1722 (2012).
[17] K. S. Novoselov, A. K. Geim, S. V. Morozov, D. Jiang, Y. Zhang, S. V. Dubonos, I. V. Grigorieva, and A. A. Firsov, Science **306**, 666 (2004).
[18] T. Stauber and N. M. R. Peres, J. Phys.: Condens. Matter **20**, 055002 (2008).
[19] R. J. H. Clark, in *Advances in Infrared and Raman Spectroscopy*, edited by R. J. H. Clark and R. E. Hester (Wiley Heyden, New York, 1984), Vol. 11, p. 95.
[20] D. Baeriswyl and A. R. Bishop, Phys. Scr., T **19**, 239 (1987).
[21] S. R. White, Phys. Rev. Lett. **69**, 2863 (1992).
[22] E. Jeckelmann and S. R. White, Phys. Rev. B **57**, 6376 (1998).
[23] E. Jeckelmann, Phys. Rev. B **66**, 045114 (2002).
[24] E. Jeckelmann and H. Fehske, Riv. Nuovo Cimento **30**, 259 (2007).
[25] K. W. Becker, A. Hübsch, and T. Sommer, Phys. Rev. B **66**, 235115 (2002); S. Sykora, A. Hübsch, K. W. Becker, G. Wellein, and H. Fehske, Phys. Rev. B **71**, 045112 (2005).
[26] S. Sykora, K. W. Becker, and H. Fehske, Phys. Rev. B **81**, 195127 (2010).
[27] J. Bonča, S. A. Trugman, and I. Batistić, Phys. Rev. B **60**, 1633 (1999).
[28] A. Alvermann, D. M. Edwards, and H. Fehske, J. Phys. Conf. Ser. **220**, 012023 (2010).
[29] C. L. Kane, P. A. Lee, and N. Read, Phys. Rev. B **39**, 6880 (1989).
[30] G. Martinez and P. Horsch, Phys. Rev. B **44**, 317 (1991).
[31] S. A. Trugman, Phys. Rev. B **37**, 1597 (1988).
[32] V. J. Emery, S. A. Kivelson, and H. Q. Lin, Phys. Rev. Lett. **64**, 475 (1990).
[33] M. Dzierzawa, in *The Hubbard Model*, edited by D. Baeriswyl, Vol. 343 of NATO Advanced Study Institute Series B: Physics (Plenum, New York, 1995).
[34] S. Ejima, F. Gebhard, and S. Nishimoto, Europhys. Lett. **70**, 492 (2005).
[35] T. Giamarchi, *Quantum Physics in One Dimension* (Clarendon, Oxford, 2003).
[36] M. Ogata, M. U. Luchini, S. Sorella, and F. F. Assaad, Phys. Rev. Lett. **66**, 2388 (1991).
[37] A. Moreno, A. Muramatsu, and S. R. Manmana, Phys. Rev. B **83**, 205113 (2011).
[38] M. Berciu and H. Fehske, Phys. Rev. B **82**, 085116 (2010).
[39] I. Bloch, J. Dalibard, and W. Zwerger, Rev. Mod. Phys. **80**, 885 (2008).
[40] A. Eckardt and M. Lewenstein, Phys. Rev. A **82**, 011606 (2010).